Electromigration in YBa$_2$Cu$_3$O$_{7-\delta}$ using a Metal Clad Near-Field Scanning Optical Microscope Probe

S. H. Huerth, M. P. Taylor, and H. D. Hallen

North Carolina State University, Raleigh, NC 27695

B. H. Moeckly

Conductus, Inc. Sunnyvale, CA 94086

Electromigration or electron-induced-migration (EIM) of oxygen in the high-temperature superconductor YBa$_2$Cu$_3$O$_{7-\delta}$ (YBCO) alters the superconducting properties through variations in the oxygen concentration. We study this process with unprecedented spatial resolution and find that the transport of oxygen through a grain boundary into a neighboring grain is unlikely, and that hot electron effects dominate the mechanism for EIM in this system. The extent of the EIM effects implies that grain boundary scattering is strong for these electrons. EIM is induced with the tunnel current from the metal cladding on a near-field optical microscope (NSOM). Variations in the oxygen concentration due to fabrication, aging, and electromigration are imaged optically and corroborated to the grain structure.

Electromigration (EM) of oxygen in YBa$_2$Cu$_3$O$_{7-\delta}$ (YBCO) has been reported in several papers.[1,2] Device quality and lifetime can be limited by it, so understanding and controlling this process is important. The change of the superconducting current-voltage curves after various EM doses was used to show improvement of microbridge critical current at low dose, degradation at high dose, and reversibility of electromigration. It was experimentally determined that a current density of 3-5 MA/cm^2 at room temperature improved the critical current while higher current densities caused degradation. EM has also been used to change the properties of superconducting Josephson junctions, although the behavior is somewhat more complex. Heating the samples in an oxygen atmosphere was found to partially reverse the EM effects.[1] EM of oxygen in YBCO arises in fault protection for electrical power systems. Excess current in a superconducting bar causes it to become normal and heat. EM ensues, resulting in the equivalent of a low insertion loss, high current fuse. EM characterization in commercial superconducting material is needed for reliability and lifetime estimates.

In this paper, we localize the electron-induced-migration (EIM) of oxygen, in samples deposited at Conductus, by using a near-field scanning optical microscope (NSOM). This improved resolution, combined with NSOM topographic images, open a new venue into EIM physics in this system. We find that we can induce EIM with tunnel electrons from the NSOM tip, that hot electrons are important in the EIM mechanism, and that grain boundary scattering is strong for these electrons. The transport of oxygen from one grain to another is found to be small. We select the local area to electromigrate -- within a grain or at a grain boundary, for example, from NSOM images. The results of the EIM are imaged with NSOM as changes in the reflectance induced by differences in the oxygen concentration. This adds another capability to NSOM, which has already been used extensively for materials analysis,[3] spectroscopy,[4,5] and electron-hole recombination time imaging.[6]

Several groups have studied the optical properties of YBCO.[7,8,9,1010] Kircher et al[10] found that the reflectance decreases with increasing oxygen content for the electric field parallel to the a-axis, but the opposite and a stronger dependence for the electric field parallel to the c-axis. Far field measurements of c-axis normal films show an anti-correlation between reflectivity and oxygen content, as has been observed.[2] The situation is not as straightforward in NSOM. Calculations[11,12] of the electric field near an NSOM probe show that the component of electric field perpendicular to the sample is similar in magnitude to that parallel to the sample. The boundary conditions imposed in NSOM for coupling light from the aperture to the detector in the reflection geometry with a conducting sample[13] favor the detection of light polarized perpendicular to the sample. Thus, we expect the stronger dependence of the electric field parallel to the c-axis[10] to dominate. There will be a positive correlation between the reflectivity and oxygen content in NSOM measurements. Our images of aged and electromigrated samples are consistent with these expectations.

The physics of EIM is very complex and has been modeled in various ways.[14,15,16,17,18] EM is usually modeled as a momentum transfer from the moving electrons in the "electron wind" to the atoms in the lattice. It can also be caused by the electrostatic force present in the material (the "direct force"). Measurements of EM of the basal-plane oxygen toward the anode, not the cathode, in YBCO[2] support the latter mechanism in lithographically-defined structures of this material, since the O(1) atoms exist as negatively charged ions. EIM induced by tunnel electrons can also be caused by hot (few eV) electron scattering, elastically or inelastically, from the oxygen atoms. YBCO is an orthorhombic lattice, with the O(1) oxygen moving in the Cu(1) planes.[19]

The sample was imaged using an NSOM in reflection mode, similar to that used previously,[20] but the shear force is detected using the tuning fork method.[21] The sample is carbon-taped to the extender tube mounted on the piezoelectric scanner. Ar^+ laser light, 514nm or 488nm, is coupled into the fiber and the light reflected from the sample focused by a 0.45 NA lens onto a photodiode. The preamplified signal is filtered to 3 Hz and averaged 5 times. The optical image from the photodiode is collected simultaneously with the topographic image. The probe apertures, resulting from an angled ~500 nm Al coating, were characterized with SEM and were less than 100nm in diameter. An image was obtained for each wavelength before and after each EIM.

EIM was induced with a negative voltage applied to the sample and using the probe as a tunneling electrode. To allow tunneling, the shear force regulation level was reduced, causing the sample to approach the tip. Once the tunnel current reached the desired level, the probe was stopped and, except for feedback dithering, held in this position from 36 minutes to 8 hours to achieve the desired dosage. The voltage applied to the sample in this study was varied from -1 to –3 volts. The laser was shut off during EIM.

The YBCO films were deposited by laser ablation onto $LaAlO_3$ substrates. A 20 nm buffer layer of CeO_2 was first grown in order to suppress *a*-axis growth. The YBCO films were grown to a thickness of 200 nm, at a substrate temperature of 785 °C, in a background oxygen pressure of 400 mTorr. The laser fluence was ~1 J/cm^2. We have grown many hundreds of YBCO films using this procedure, and the process produces routinely excellent films, as discussed in previous publications.[22] These films typically possess a room-temperature resistivity of ~200–250 $\mu\Omega$ cm which decreases linearly with decreasing temperature and extrapolates to zero at 0 K. Superconducting transition temperatures are typically above 89–91 K with transition widths less than 1 K. Standard 2θ X-ray diffraction analysis of the films in this study
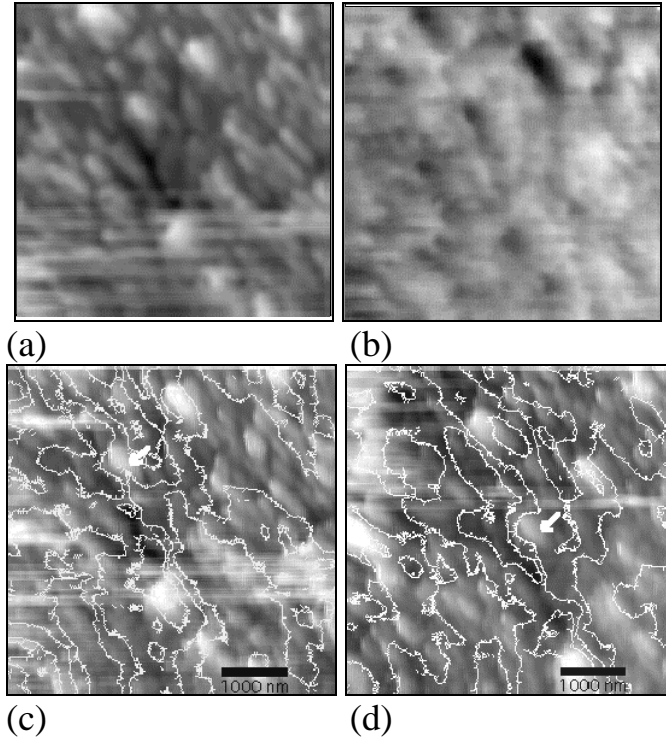
(a)

(b)

(c)

(d)

Figure 1: Representative images of YBCO in a 5 micron square region. (a) The topography is shown with a 150 nm range of the gray scale (white higher). (b) The corresponding optical (green) image with a 6 nW range (~43 nW average value, white lower reflectivity, higher oxygen content)). (c) An overlay of (a) in gray scale and (b) as a contour plot to illustrate the correlation between the grains and oxygen content before EIM. The tick marks on the contours point towards lower oxygen content. (d) As (c) but using the after EIM and optical images. The images are shifted due to microscope drift. The white arrow shows a major path of oxygen flow during the EIM as the contour has shifted across the grain pointed to.

indicated the presence of only (00*l*) peaks. Scans of the (104) χ-angle confirmed that the films were entirely *c*-axis oriented with no detectable amount of *a*-axis-oriented grains. In addition, φ-scan analysis indicated that the films were completely oriented in the *a-b* plane, i.e. high-angle grain boundaries were absent.

We characterize the initial surface with the simultaneously acquired topographic and optical images from the NSOM. Figure 1(a) shows a 5 micron square topographic scan on one of the samples used. Figure 1(b) is the corresponding optical data taken with 514 nm light, displaying magnitude variations due to reflectivity changes. Since the films are uniform, the optical variations are likely due to changes in oxygen content. The optical image shows some correlation with the topographic grains. This is not a topographic induced artifact in the optical image, since the effect remains well away from the grain edges in this slow (due to high signal averaging) scanned data. It appears that the oxygen content varies from one grain to another. An overlay of the optical contours over the topographic gray scale illustrates this. Many of the topographic features appear outlined. This correlation is not, and isn't expected to be, one-to-one. Rather, the oxygen content varies primarily between grains when it does vary. Most grains sticking out of the surface have a significantly lower near-surface oxygen concentration than the rest of the sample (NSOM is surface-dominated). This suggests that oxygen can move within the ab-plane at room temperature much more readily than it can in the c-direction. It also suggests that oxygen can escape from the sample by diffusing laterally to the exposed edges of the ab-planes in these regions extending 6-70 nm above the surface plane. The uniformity within the grains and differences between some grains imply that the motion of oxygen through at least some grain boundaries is inhibited. Nothing can be said about the motion along grain boundaries from these measurements, although other data suggest mobility in that direction.

We next demonstrate EIM with the tunnel current. For the sample shown in Figure 1, EIM was induced by applying –1 V to the sample, and decreasing the tip-sample distance until a current of 2 nA was achieved. The system was left in this state for 36 minutes. The changes during EIM can be related to the grain structure by comparison of Figure 1(c and d). Since the topography remains unchanged, it is likely that oxygen motion is responsible for the changes. Oxygen was forced into the grain that sticks out of the surface. One might have expected a region of reduced oxygen content to encircle the grain, indicating the oxygen source. The fact that none is observed indicates either a diffuse source for the oxygen, or that the oxygen moves from the bulk of the film
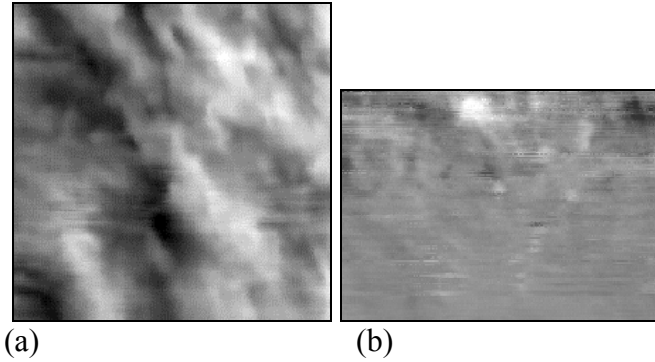

(a) (b)

Figure 2: (a) Optical image of the region shown in Figure 1 but taken with blue (488 nm) light, 10 nW range, before EIM. (b) The difference image obtained after that shown in (a) was shifted and subtracted from the blue optical image taken after EIM with 12 nW range. Note that the region shown is smaller, 3.9×2.9 µm, since only the overlapping regions of the scans are meaningful.
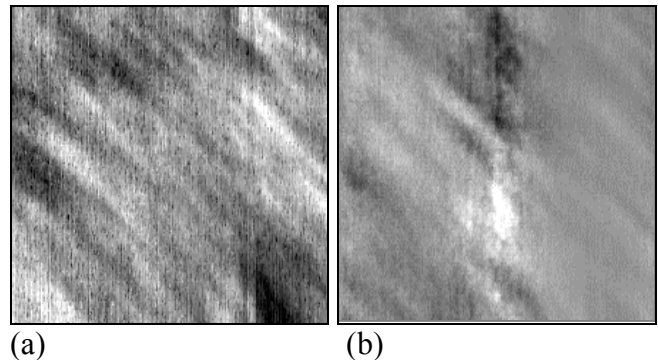
towards the surface. The position of the arrows on the figure indicates the direction of contour line motion during the EIM process. Comparisons of the images in this way gives good insights into the granular dependence of the EIM, but does not provide an ideal method for measuring the size of the effect. The variation in the native oxygen concentration of the samples with position also hinders this measurement. The size of the effect can be measured readily in 'after' minus 'before' optical difference images. We therefore performed cross-correlation between the before and after *topographic* images to quantify the lateral drift over the several hours between the two images, during which several other images and the EIM occurred. The shift given by this correlation agrees with that from the correlation of the two optical images to within one pixel. The measured drift rate was 260 nm per hour. Intensity variations between the optical images were corrected by scaling before subtraction. A similar shift and subtraction was performed with the topographic images before and after electron-induced-migration. The result showed only noise. We have not observed any evidence of topographic changes during the EIM of the oxygen. Figure 2 shows these results for the same region as shown in Figure 1, but as imaged with 488 nm light. The radius of the effected area is 250 nm. The results from a different sample, electromigrated for 8 hours at -3V and 3nA, are shown in Figure 3. It is interesting to note that the radius of the effected region is still approximately 250 nm despite the much stronger EIM driving force.

(a) (b)

Figure 3: (a) Optical image of a 10 µm square region of a sample taken with green (514 nm) light, before EIM, with 1 nW range. (b) The difference image obtained after that shown in (a) was shifted and subtracted from the green optical image taken after EIM. The 9 µm square overlapping region is shown.

The size of the effect should depend upon the region for which the force is sufficient to move oxygen atoms. First, we note that there should be no effect due to local heating of the sample since the local temperature rise is extremely small. The energy input by the tunnel electrons is a few tens of nanowatts (similar to that of the light), and the heat diffuses into three dimensions, due to the small source size. Diffusion calculations[23] show that the temperature rises by many orders of magnitude less than it does with a larger spot. The force due to the current density falls as the current spreads out, eventually dropping as 1/distance for a thin film. A prediction of the size of the EIM-affected region, using current density requirements from the literature, yields a radius much smaller than we observe. Our configuration differs from prior work in that we inject few-volt electrons directly into the EIM region rather than locally increasing the current density of near-thermal-energy electrons through lithographic constriction of the conductor[1,2]. This means that we inject the electrons with a higher momentum, due to the increased local potential drop. It is likely that this voltage effect plays a major role in this process, as it has in other few-eV-electron-induced processes.[24,25,26] In those previous studies of metallic films, the size was found to be limited by growth dynamics, and eventually the grain size, since the grain boundary strongly back- or inelastically-scattered the hot electrons. The figures support a similar conclusion here, although for motion of different components in a very different materials system. The size of the affected region after small doses should be dose-dependent, but at higher doses limits to a size given by either the grain size or the inelastic scattering length of the injected electrons. The grain size limitation, as suggested in Figure 1, would imply that elastic or inelastic scattering confines the hot electrons to a single grain in this material also. The grain size limit would also tend to disfavor a pure electrostatic origin of the electron-induced-migration, as the electric field should persist across a grain boundary.

We have shown that electrons injected from a near-field metal clad probe can induce oxygen movement over significant distances in YBCO. Our images show changes in the reflectivity corresponding to a change in the oxygen concentration where the EIM occurred. The results suggest that hot electrons injected into YBCO remain confined to a single grain, at least until they lose sufficient energy such that they are unable to induce oxygen motion. No topographic changes are observed during the electron-induced-migration. The local variations in the oxygen concentration of the as-grown surfaces show that diffusion of oxygen at room temperature occurs primarily in the ab-plane and within a grain.

[1] B. H. Moeckly, D. K. Lathrop, and R. A. Buhrman; Phys. Rev. B, **47** (1), 400-417 (1993).

[2] B. H. Moeckly, R. A. Burhman, P. E. Sulewski, Appl. Phys. Lett. **64**, 1427 (1994).

[3] H. D. Hallen, A. La Rosa, and C.L. Jahncke; Physica Status Solidi (a) **152**, 257-268 (1995).

[4] C.L. Jahncke, M. A. Paesler, and H.D. Hallen; Appl. Phys. Lett. **67** (17), 2483-2485 (1995).

[5] C.L. Jahncke and H. D. Hallen, 9th annual meeting of IEEE Lasers and Electro-Optics Society (LEOS) 96 conf. Proc. Vol. **1**, pp. 176-177.

[6] A.H. La Rosa, B. I. Yakobson, H.D. Hallen; Appl. Phys. Lett. **70** (13), 1656-1658 (1997).

[7] P.E. Sulewski, T. W. Noh, J. T. McWhirter, A. J. Sievers, S. E. Russek, R. A. Buhrman, C. S. Jee, J. E. Crow, R. E. Salomon, and G. Myer, Phys. Rev. B **36** (4), 2357-2360 (1987).

[8] G. Zhao, Y. Xu, W.Y. Ching, K. W. Wong; Phys. Rev. B, **36,** 7203 (1987).

[9] K. Kamaras, C. D. Porter, M. G. Doss, S. L. Herr, D. B. Tanner, D. A. Bonn, J. E. Greedan, A. H. O'Reilly, C. V. Stager, and T. Timusk, Phys. Rev. Lett. **59** (8), 919-922 (1987).

[10] J. Kircher, M. K. Kelly, S. Rashkeev, M. Alouani, D. Fuchs, and M. Cardona, Phys. Rev. B, **44**, 217-224 (1991).

[11] H.A. Bethe, Phys. Rev. **66**, 163 (1944).

[12] C.J. Bouwkamp, Phillips Research Report **5**, 401 (1950).

[13] M.A. Paesler and P.J. Moyer, "Near-Field Optics: Theory, Instrumentation and Applications," (John Wiley and Sons, Inc., New York, 1996).

[14] K. P. Rodbell, M.V. Rodriguez, and P. J. Ficalora; J. Appl. Phys. **61** (8), 2844-2848 (1986).

[15] M.L. Dreyer, K.Y. Fu, and C.J. Varkar; J. Appl. Phys. **73** (10), 4894-4902 (1993).

[16] K. Hinode, T. Furusawa, and Y. Homma; J. Appl. Phys. **74** (1), 201-206 (1993).

[17] H. Boularot and R. M. Bradley; J. Appl. Phys. **80** (2), 756-761 (1996).

[18] J. R. Lloyd; Semicond. Sci. Technol. **12**, 117-1185 (1997).

[19] J. B. Goodenough and A. Manthiram; Proceedings of the IX Winter meeting on Low Temperature Physcis: *High Temperature Superconductors* (1988).

[20] C.L. Jahncke and H.D. Hallen, Rev. of Sci. Instr, **68** (4), 1759 (1997).

[21] Khaled Karrai and Robert D. Grober, Appl. Phys. Lett. **66**, 1842 (1995).

[22] B. Moeckly and K. Char, Physica C **265**, 283 (1996).

[23] A.H. LaRosa, C.L. Jahncke and H.D. Hallen; SPIE Proc. **2384**, 101 (1995).

[24] H.D. Hallen, A. Fernandez, T. Huang, R.A. Buhrman, and J. Silcox, Phys. Rev. Lett. **69**, 2931 (1992).

[25] H.D. Hallen and R.A. Buhrman in *Atomic and Nanometer-Scale Modification of Materials: Fundamentals and Applications*, edited by Ph. Avouris (Kluwer, Dordrecht, 1993).

[26] H.D. Hallen, in *The Technology of Proximal Probe Lithography*, edited by Christie Marrian, Vol. IS10 (SPIE, Bellingham, 1993).